Shoot scattering phase function for Scots pine and its effect on canopy reflectance

Matti Mõttus[*,a], Miina Rautiainen[b], Michael E. Schaepman[c]

[a]*Department of Geosciences and Geography, University of Helsinki, P.O. Box 64, FI00014 Finland*
[b]*Department of Forest Sciences, University of Helsinki, P.O. Box 27, FI00014 Finland*
[c]*Remote Sensing Laboratories, Department of Geography, University of Zurich, Switzerland*

Abstract

Spectral and directional reflectance properties of coniferous forests are known to differ from those of broadleaf forests. Many reasons have been proposed for this, including differences in the optical properties of leaves and shoots, the latter being considered the basic unit in radiative transfer modeling of a coniferous canopy. Unfortunately, very little empirical data is available on the spectrodirectional scattering properties of shoots. Here, we present results of angular measurements (using an ASD FieldSpec 3 spectroradiometer mounted on LAGOS) of ten Scots pine shoots in the spectral range 400–2000 nm. The shoots were found to scatter anisotropically with most of the radiation reflected back into the hemisphere where the radiation source was positioned. To describe the measured directional scattering pattern, we propose a phase function consisting of isotropic and Lambertian scattering components. Next, we used the proposed scattering phase function in a Monte Carlo radiative transfer model. Angular reflectance of a modeled horizontally homogeneous shoot canopy has, due to shoot scattering anisotropy, an enhanced "dark spot" as compared with a canopy composed of isotropic scatterers and a quantitatively similar leaf canopy.

Key words: Radiative transfer in vegetation canopy, Pinus sylvestris, scattering phase function, dark spot

1. Introduction

Coniferous canopies have several distinct structural features, and therefore, impose modifications on radiative transfer models originally formulated for broadleaved canopies. Basic concepts needed in radiative transfer modeling, such as leaf area index (LAI) and *G*-function (mean projection area of unit one-sided leaf area in any given direction) were originally defined for flat leaves. When they are applied to non-flat conifer needles, reformulations are needed. For example, by using hemisurface area instead of one-sided leaf area (e.g. Chen and Black, 1992; Stenberg, 1996), the equations defined for a leaf canopy can be applied to a needleleaf forest. However, such reformulations correct only for the different shapes of the smallest canopy scattering units, i.e., leaves and needles. Additionally, conifers and broadleaves differ significantly with respect to small-scale structure: conifer needles are grouped into shoots.

Coniferous canopy light interception models have used the shoot as the basic structural element for a long time (e.g. Oker-Blom and Kellomäki, 1983; Nilson and Ross, 1997; Cescatti, 1997). Similarly, shoot-level clumping is accounted for in forest reflectance models. However, besides altering the amount of radiation intercepted by trees, grouping of needles into shoots also affects the way non-absorbed radiation is scattered by a vegetation canopy. The effect of shoot-level clumping on scattering phase function (the function describing the directionality of radiation scattering) has not yet been implemented in canopy radiative transfer models (Rochdi et al., 2006; Stenberg et al., 2008). Precise knowledge of shoot scattering phase function and shoot albedo will substantially improve radiative transfer-based canopy reflectance models. In particular, knowledge of shoot albedo will allow us to use it as a coupling element between needle optical properties and canopy scattering.

Empirical data on the scattering properties of coniferous shoots, i.e. the shoot scattering phase function for different species, are crucial for an improved parameterization of radiative transfer models applied in coniferous areas, for inverting canopy reflectance measurements or estimating radiation absorption. However, very little has been published about the spectral properties of coniferous shoots.

Measuring the directional properties of conifer shoots is a difficult task and a multidimensional problem. A coniferous shoot is a three-dimensional object and to measure all points on its surface from the same angle, the distance from the radiometer to the shoot has to be much larger than the shoot dimension itself. The field-of-view (FOV) of the radiometer has to be uniform: radiation scattered by different parts of the shoot has to be registered with uniform sensitivity. Also, the shoot has to be irradiated by a uniform, spectrally continuous and powerful beam as the absorption of a shoot varies from almost 100% at red wavelengths to close to zero in the near-infrared. Shoot scattering anisotropy adds another order of magnitude to the range of variation of the scattering signal. The light source should illuminate the shoot with negligible internal divergence, preferably it should produce a collimated beam. Finally, to obtain shoot albedo, directional measurements must cover the full sphere, a

[☆]Published in Agricultural and Forest Meteorology, doi: 10.1016/j.agrformet.2011.10.012
[*]Corresponding Author
Email address: matti.mottus@helsinki.fi (Matti Mõttus)

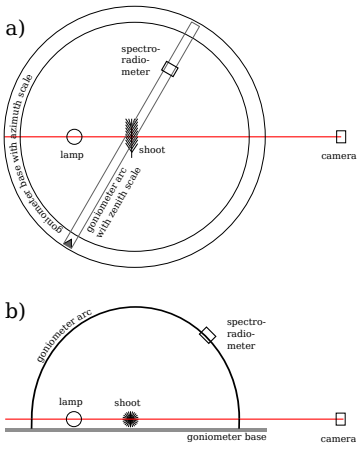

Figure 1: The measurement setup as viewed from a) above and b) side. Diagram not to scale.

solid angle of 4π.

Previously, Ross et al. (1994) carried out angular multispectral measurements of the bidirectional reflectance distribution function (BRDF) of Scots pine (*Pinus sylvestris*) shoots. Due to the limitations of the measurement apparatus, measurements were performed in a single plane only and the results could not be integrated to obtain shoot scattering coefficient, or the shoot albedo ω_{SH}. Using these measurements, Nilson and Ross (1997) presented a radiative-transfer based approach for modeling the reflectance properties of a shoot canopy. However, a direct validation of the theory is still missing, mainly due to lack of empirical data. Additionally, several Monte Carlo radiation transfer simulation results have been published which display detailed complex scattering patterns as functions of the angles between the shoot axis, illumination and observation directions (e.g., Smolander and Stenberg, 2003; Rochdi et al., 2006). These Monte Carlo simulations, however, have ignored the specular reflectance component and made simplifying assumptions on needle shape and shoot geometry.

In this paper, we report a laboratory-based experimental design for measuring the scattering phase function of coniferous shoots and demonstrate its feasibility using Scots pine shoots. We analyze the directional scattering measured for these shoots and test simple scattering phase functions against our empirical data. Next, we use a Monte Carlo model to predict the reflective properties of horizontally homogeneous canopies consisting of phytoelements with three different phase functions parameterized using our measurement results. Finally, we discuss the implications of our results on inverting remote reflectance measurements made above coniferous canopies.

2. Materials and methods

2.1. Instrumentation

The measurements were performed using the LAGOS geometer system (Dangel et al., 2003, 2005) in April 2011. The goniometer system facilitated measuring of radiation scattered by an object located in its center into almost any direction in the upper hemisphere. While the azimuth range of the system covered the full circle, the maximum zenith angle was limited by construction to 74°. The accuracy of determining the view zenith and azimuth angles was better than 1°. The radius of the arc of the goniometer corresponding to the distance between the sample (in our case, a pine shoot) and the spectroradiometer was 2.00 m. The goniometer was installed in a dark room with spectrally neutral black walls. The floor inside the goniometer arc was covered by black plates. A schematic presentation of the setup is given in Fig. 1.

The spectra were recorded with an ASD FieldSpec 3 spectroradiometer with no foreoptics (Milton et al., 2009). The spectroradiometer covered the spectral range from 350 to 2500 nm with a spectral resolution of 3 nm at 700 nm and 10 nm at 1400 and 2100 nm. Thus, the area in the center of the goniometer corresponding to the field-of-view (FOV) of the instrument was much larger than the projected area of a shoot. This configuration was chosen due to the non-uniformity of the FOV of the FieldSpec (MacArthur et al., 2007). The receiving surface of the instrument was an open end of a bundle of optical fibers used to transmit the radiation to the sensors. However, the individual fibers of an ASD instrument are oriented at small angles to the optical axis and tend to see slightly different areas around the center of the FOV. Clearly, this causes problems when measuring non-uniform objects such as shoots on a contrasting background. By ensuring that the signal originates only from the very center of the FOV close to the optical axis, the non-uniformity was significantly reduced. The uniformity of the FOV in the small solid angle containing the shoot was verified by rotating the open end of the optical cable while keeping it centered at the shoot. Doing so, we observed only slight variations in the spectral radiance recorded by the instrument. To decrease the signal caused by stray light, a view limiting tube made of black cardboard was attached to the fiber, restricting its FOV to approximately 15°. This angle was chosen to guarantee the full visibility of the shoot in spite of the possibility of small alignment errors. As a drawback compared to using foreoptics (such as the standard 8-degree lens limiting the FOV to about twice the projected area of a shoot), a significant amount of radiant power was lost.

The spectrometer was used in digital number mode, i.e. the output of the instrument was not converted into radiometric units. Instead, we used a relative measurement scheme: before and after measuring the scattering properties of a shoot, we measured the signal reflected by a 2-inch calibrated Spectralon white reflectance panel. Similarly to the pine shoots, the projected area of the panel was much smaller than the FOV of the spectroradiometer. The panel was attached to a tripod and carefully oriented to be perpendicular to the incident radiation beam. The rod attaching the panel to the tripod was covered with spectrally neutral black canvas. The small contribution of the attachment system was measured after removing the panel and corrected for during data processing.

We used a brightness-stabilized quartz tungsten halogen lamp and lens system (manufactured by Oriel, type 6317) as the radiation source. An aspherical reflector in combination with a Köhler illuminator and a condenser secured spectral and radia-

tion inhomogeneities of the projected beam to be less than 2%. The lamp was located in the horizontal plane of the center of the goniometer with the latter being in the center of the beam. The diameter of the beam in the lamp window was about 4 cm and the divergence of the beam (half-vertex angle) was 12°. The distance of the lamp window from the center of the goniometer was 80 cm. Thus, the diameter of the light cone at the location of the shoot (∼ 40 cm) was considerably larger than any shoot dimension, i.e. the shoot was completely irradiated during the measurements.

In addition to radiometric measurements, the projection area of the shoot had to be determined. For this purpose, we used a 12-megapixel Nikon D90 digital camera mounted on a tripod at a distance of about 4 m from the shoot on the optical axis.

2.2. Measurements

We used a simple two-dimensional quadrature on the sphere to measure the directional reflectance properties of a shoot. Azimuth was sampled at equal steps in its compete range (360°) while the polar angle values ϑ_i were chosen so that $\cos\vartheta_i$, $0 < \vartheta_i < 180°$, are the Gauss-Legendre nodes on $[-1, 1]$. We selected a quadrature with six nodes, but as the goniometer allowed to sample only one hemisphere at a time, just three zenith angles were used for each azimuth value: 21.2°, 48.6°, and 76.2°. In practice, the maximum zenith angle achievable by the goniometer was about 74°. We assumed that within the general accuracy of the experimental setup, the two-degree difference was negligible. There were two additional limitations to the measurable angle range. Measurements in the principal plane (azimuth angles 0 and 180°), $\vartheta = 74°$ was not achievable as in the backscattering position, the shoot was blocked by the lamp; in the forward scattering direction, the sensor was in the direct light beam which masked the weaker scattered signal.

Stray light (i.e., signal with no shoot) was measured for all directions in the quadrature. To reduce the noise present in the data, standard Savitzky-Golay filtering was applied to stray light data separately for each direction. The spectrally smoothed stray light signal was subtracted from each measurement before further processing. The spherically integrated contribution of stray light was usually below 5% of the scattered signal for a shoot for wavelengths between 400 and 1800 nm. In ultraviolet and the longwave end of SWIR spectral region, stray light occasionally exceeded 10%.

The number m of the azimuth angle nodes ϕ_i used was 12, i.e., double the number of polar angle nodes. This corresponds to an azimuth angle step of 30°. The weights corresponding to each measurement angle (ϑ_i, ϕ_j) were $W_{ij} = \pi w_i/m$, where w_i is the Gauss-Legendre weight corresponding to the polar angle ϑ_i. This quadrature provides reasonable accuracy for integrating over 4π (e.g., Atkinson, 1982) . The chosen quadrature suited well the construction of the goniometer: after fixing the azimuth angle, the measurements for the polar angles in one hemisphere could be made in a fast succession. For the missing directions in the quadrature, interpolation was used. For the missing scattering measurement in the backward direction, i.e., in the direction closest to the hotspot, we used the largest value recorded in four closest neighboring nodes. For the missing direction close to forward scattering, the average signal of its four closest neighbors was used.

The shoot was fixed in the center of a specially designed shoot holding frame using ordinary black sewing thread. The frame consisted of a metal ring with a diameter of 1.0 m with four handles in cardinal directions to allow fast attachment and rotation by a fixed angle. The shoot was attached with its axis in the plane of the frame and approximately horizontal. The frame with the attached shoot was placed in the orthogonal plane (normal to direction of the light beam) in the middle of the goniometer arc so that the shoot was always irradiated from its longest side, maximizing radiation interception. The goniometer was then used to measure the scattered signal in one hemisphere. Next, the frame was rotated 180° while not changing the irradiated side of the shoot and re-centered within the light beam. After completing the measurements in the second hemisphere, we had covered the solid angle of 4π.

The observation geometry described above meant that the frame was in one of the measurement planes corresponding to $\phi = 90°$ and $\phi = 270°$, thus blocking the spectroradiometer's view in this plane. To avoid this, we used the average of the scattering at $\phi = 80°$ and $\phi = 100°$ as an estimate for scattering at $\phi = 90°$. Similarly, the average signal of $\phi = 260°$ and 280° was used for $\phi = 270°$.

We allowed the spectroradiometer to warm up for a sufficient amount of time (always more than 1h). Dark current was measured at approximately three minute intervals before each scan over the zenith angle. Due to the low signal levels caused by a small (compared with the FOV of the instrument) dark target on a black background, the radiation collection settings were set close to the sensitivity limits of the instrument: integration time for the VNIR (visual and near-infrared radiation) region was set to 1.09 s, the gains for the two SWIR (shortwave infrared) sensors were set to 8. Five spectra were averaged for each measurement direction.

After measuring the scattering signal in each hemisphere, the shoot was photographed to obtain its projection area perpendicular to the direction of incident radiation. A diffusely illuminated screen was placed between the shoot and the lamp. A scale was placed next to the shoot to enable accurate measurement of the physical dimensions of the shoot from the image. Images were stored in 12-bit raw format and processed with ImageJ (version 1.44) software to obtain intercepting areas.

2.3. Sampled shoots

Ten Scots pine shoots were collected from the vicinity of the Irchel campus of University of Zurich in March 2011. Shoots were selected visually to cover a reasonable range of their natural variation. Only the youngest shoots corresponding to the previous year's growth were selected. Within the sample, the length of the twig inside the shoot was between 6 and 17 cm, the number of needles varied between 98 and 226. Basic characteristics for all ten shoots are given in Table 1, silhouettes of the shoots are presented in Fig. 2.

Table 1: The basic structural characteristics of the measured shoots: length of the twig of the shoot, the number of needles comprising the shoot, mean needle length, and the irradiated silhouette area.

shoot number	1	2	3	4	5	6	7	8	9	10	Mean
twig length (cm)	14.8	6.1	10.9	10.4	13.7	13.6	16.8	7.7	8.3	9.2	11.2
no. of needles	194	98	170	132	226	144	198	148	100	110	152
mean needle length (cm)	6.6	4.7	5.8	6.3	4.8	5.7	5.7	6.8	6.8	6.7	6.0
silhouette area (cm²)	63.5	22.5	45.4	46.3	50.3	43.3	51.2	43.8	34.3	35.5	43.6

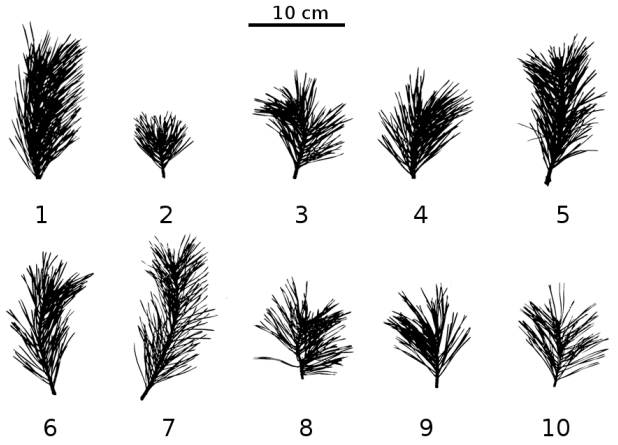

Figure 2: Silhouettes of the measured shoots recorded with a digital camera.

2.4. Analysis

We fitted three simple scattering directionality models (also known as shoot scattering phase functions) to the measured directional scattering signal. The goodness of model fit was characterized using the root mean square difference defined as

$$\mathrm{RMSD} = \sqrt{\frac{1}{4\pi}\int_{4\pi}\left[\frac{S(\Omega)}{S_{id}(\Omega)} - \omega_{SH}P_{SH}(\Omega)\right]^2 d\Omega} = \sqrt{\frac{1}{\sum_{i=1}^{N} W_i}\sum_{i=1}^{N} W_i\omega_{SH}^2\left[P(\Omega) - P_{SH}(\Omega)\right]^2}, \quad (1)$$

where $S(\Omega)$ is the measured spectral signal in the direction Ω, $S_{id}(\Omega)$ is the theoretical signal produced by an isotropically scattering non-absorbing sphere with an interceptance area equal to that of the actual shoot, $P_{SH}(\Omega)$ is a shoot scattering phase function model ($\int_{4\pi} P_{SH}(\Omega)d\Omega = 4\pi$), ω_{SH} is shoot spectral albedo, Ω_i is a direction in the quadrature, W_i is the corresponding quadrature weight, and $N = 72$ is the total number of quadrature nodes.

$$P(\Omega) = \frac{S(\Omega)}{\omega_{SH}S_{id}(\Omega)} \quad (2)$$

is the empirical phase function obtained from measurement results. $S_{id}(\Omega)$ was calculated using the reference panel measurements and photographically determined projected shoot area.

Three $P_{SH}(\Omega)$ shapes were tested against the measured directional scattering signal: isotropic, Henyey-Greenstein, and isotropic-Lambertian phase functions.

The isotropic phase function is mathematically written as

$$P_{ISO}(\Omega) \equiv 1. \quad (3)$$

In case of isotropic scattering, just a single parameter, the shoot spectral albedo ω_{SH}, is used to predict the scattered signal for any incident radiation field conditions.

The Henyey-Greenstein phase function is given as

$$P_{HG}(\Omega) = \frac{1-g^2}{\sqrt{(1+g^2-2g\cos\vartheta)^3}} \quad (4)$$

(Henyey and Greenstein, 1941), where ϑ is the scattering angle (angle between Ω_{in} and Ω corresponding to the directions of photon travel before and after scattering, respectively) and g ($-1 \le g \le 1$) is a parameter describing the directionality of scattering. Eq. (4) is a popular empirical single-parameter model used to describe scattering in various media. With the addition of shoot albedo ω_{SH}, we obtained a simple two-parameter model for describing directional shoot scattering.

The isotropic-Lambertian scattering phase function is based on the analysis of the measured anisotropy of shoot scattering. It is a superposition of two simple common scattering phase functions: isotropic scattering and Lambertian reflection:

$$P_{IL}(\Omega) = \begin{cases} f_{iso}, & \cos(\Omega_{in},\Omega) > 0 \\ f_{iso} + 4\,f_{Lamb}\,|\cos(\Omega_{in},\Omega)|, & \cos(\Omega_{in},\Omega) < 0 \end{cases}, \quad (5)$$

where f_{iso} and f_{Lamb} are the fractions of isotropic and Lambertian scattering, respectively, $f_{iso} + f_{Lamb} = 1$. The normal of the imaginary surface producing the Lambertian component is opposite to the direction of incident radiation. The factor 4 in the Lambertian scattering term of Eq. (5) for backward scattering ($\cos(\Omega_{in},\Omega) < 0$) is a result of normalization. Similarly to the case of Henyey-Greenstein phase function, use of Eq. (5) requires specification of two parameters.

We used a simple Monte Carlo model to predict the reflective properties of canopies consisting of objects (in our case, shoots) with different scattering phase functions. The modeled scene consisted of a horizontally infinite and homogeneous layer. The physical dimensions of shoots were ignored and the mean free paths of photons were generated assuming exponential attenuation of radiation (i.e., a turbid medium approach). No hot-spot corrections were applied. Only direct collimated incidence was

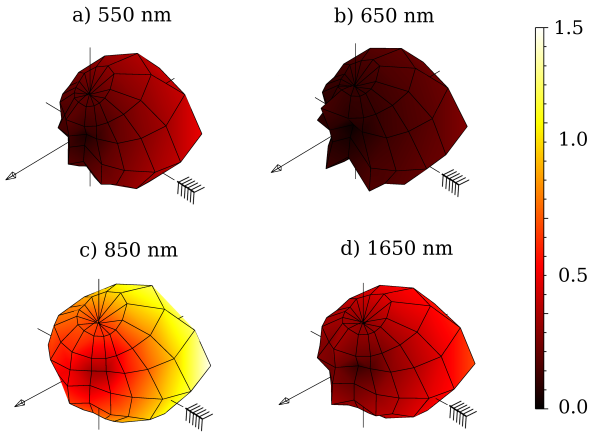

Figure 3: The scattering phase function $P(\Omega)$ for a typical shoot (number 6 in Table 1) at four wavelengths (550, 650, 850, 1650 nm). Contours indicate the shape of the phase function, colors indicate the amount of scattering in each direction (the scale indicates values of $\omega_{SH}P(\Omega)$). Arrow in each subplot indicates the direction of incident radiation. The small shoot symbol is drawn next to the axis corresponding roughly to the axis of the shoot.

assumed and the canopy was bounded from below by a totally absorbing surface.

Due to low irradiance levels and decreasing spectroradiometer sensitivity, we limited our analysis to the spectral interval between 400 and 2000 nm. While removing the potentially interesting shortwave spectral region between 2 and 2.5 microns, we were still able to completely cover the visible, near-infrared and some shortwave-infrared wavelengths.

To overcome the problems related to high noise levels, we decided to evaluate scattering directionality parameterizations based on their ability to fit the signals simultaneously for all shoots and all scattering directions instead of focusing on individual shoot phase functions. After combining the phase functions of all ten shoots, we calculated the root mean square difference (Eq. 1) between the measurements and the three fitted scattering models (Fig. 4). For the Henyey-Greenstein and isotropic-Lambertian phase functions, the additional parameter was fitted by minimizing RMSD value separately for each shoot and each wavelength to allow for between-shoot structural variations.

3. Results and discussion

The scattering phase function for a single shoot with mean structural properties (shoot 6 in Table 1) at four wavelengths (green, wavelength 550 nm; red, 650 nm; near-infrared, 850 nm; shortwave-infrared, 1650 nm) in Fig. 3. Hereafter, we concentrate our analysis on the averaged performance of the three fitted scattering phase functions. Nonetheless, Fig. 3 can be used to illustrate some general qualitative comments. For all wavelengths presented in Fig. 3, the shoot is a strong backscatterer. Contrary to what was reported by Ross et al. (1994) in their Fig. 2, we did not record a strong and wide (up to 60° from Ω_{in}) forward-scattering peak. Although we could not measure in the exact forward-scattering configurations, such a wide peak would have affected measurements at neighboring quadrature nodes. A particular feature present in all the subplots of Fig. 3 is a dark spot facing the viewer. The figure is laid out in a way that the axis of the shoot lies approximately along the second horizontal axis (marked with a small shoot symbol in Fig. 3) with attached end of the shoot pointing away from the viewer. The dark spot is associated with seeing needle tips pointing in the direction of the viewer in the dark, forward-scattering hemisphere. The flattening of the phase function in the vertical direction visible in Fig. 3 is most likely caused by the shoot holding frame being inside the FOV of the radiometer. However, the angles corresponding to the vertical axis in Fig. 3 were not used in the quadrature for calculating shoot scattering or RMSD (Eq. 1) and are only presented here as an illustration.

The phase function shapes for wavelengths where the shoot absorbs little (850 and 1650 nm) are relatively smooth. High level of noise is evident as the spikes in $P(\Omega)$ for the 650 nm (red) and, to a lesser extent, also 550 nm (green) wavelengths. The noise present in each directional scattering measurement (due to working at the sensitivity limit of the ASD spectroradiometer) was further amplified by removing stray light and normalizing the signal to Spectralon reflectance, both of which also were also inevitably noisy.

Potential heat emissions from the radiation source could have an effect on the optical properties of the needles and thus, our goal was to keep the measurement time for each shoot and view angle as short as possible. Although direct heat flux from the lamp is decoupled using a condenser and although needles are covered by a relatively thick wax layer, exposing a cut-off shoot to a strong radiation source at a relatively close distance will inevitably lead to water loss and changes in its biochemical composition over time. To monitor shoot health, we calculated the red-edge inflection point from each recorded spectrum. We did not detect a dependence between the location of the inflection point and time elapsed from the beginning of the measurements. Therefore, we consider spectral changes related to shoot biochemical changes as minimal.

The isotropic-Lambertian shoot scattering model produces clearly the smallest RMSD values across the spectrum while isotropic approximation expectedly performs worst (Fig. 4). The two-parameter Henyey-Greenstein phase function is between the two other models with regard to its RMSD, capturing to some extent the directionality of shoot scattering.

The isotropic-Lambertian function was chosen after noticing that in backward-scattering directions ($\cos(\Omega_{in}, \Omega) < 0$), the reflected signal depended strongly on the view angle. To quantify the relevance of the non-isotropic scattering component, we analyzed the regression coefficient (i.e., the slope of the regression line) of measured signal and $\cos(\Omega_{in}, \Omega)$ for all wavelengths separately in the forward- and backward-scattering directions. More precisely, we calculated the statistical level of significance α for obtaining a regression coefficient as different

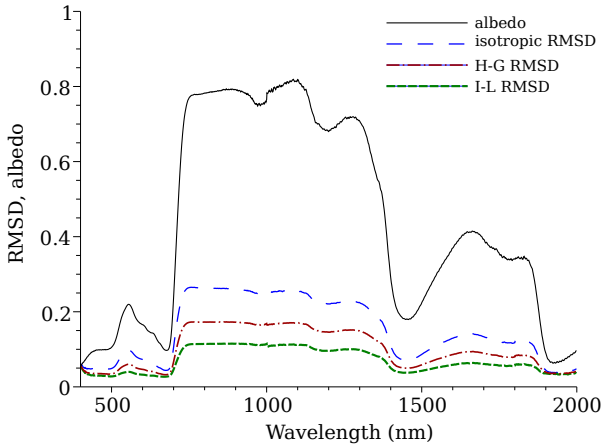

Figure 4: Average spectral shoot albedo (solid line) for the ten measured shoots together with the spectral dependence of root mean standard difference (RMSD) for isotropic phase function (Eq. 3, long dashes), Henyey-Greenstein phase function (Eq. 4, H-G, dash-dot), and isotropic-Lambertian phase function (Eq. 5, I-L, short dashes).

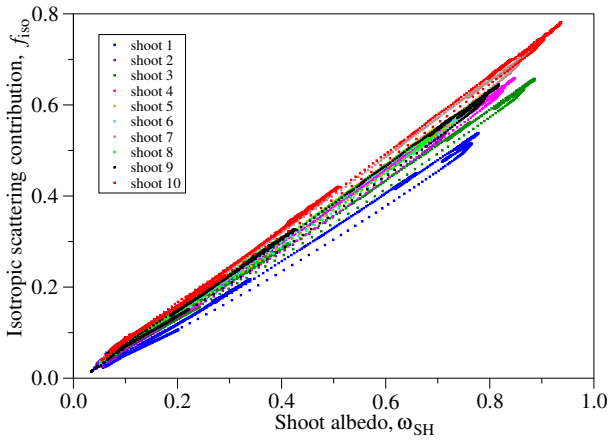

Figure 5: The contribution of isotropic scattering f_{iso} as a function of shoot albedo ω_S according to the isotropic-Lambertian model. Shoots are plotted with different colors.

from zero as the value resulting from our measurements.

For the backward-scattering directions, we almost universally found a clear linear dependence between scattering in the direction Ω and $\cos(\Omega_{in}, \Omega)$. For most wavelengths between 400 and 2000 nm, α was below 0.05. However, the level of significance varied with shoot albedo: for $\omega_{SH} < 0.15$, the regression tended to be less significant (i.e., $\alpha > 0.1$, results not shown here).

In the forward-scattering directions, however, the level of significance was much larger (generally $\alpha \gtrsim 0.6$) regardless of ω_{SH}, indicating a lack of correlation. Still, it is clear that there can be no abrupt change at the scattering angle of 90° ($\cos(\Omega_{in}, \Omega) = 0$). P_{SH}, averaged over shoot orientations, may be assumed to be a monotonously increasing (instead of non-decreasing as defined by the isotropic-Lambertian model) function of the scattering angle (Ω_{in}, Ω). Additionally, despite its good performance, isotropic-Lambertian model is an empirical

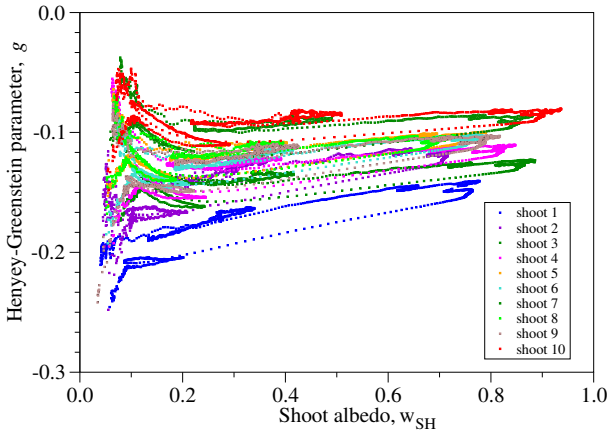

Figure 6: The Henyey-Greenstein scattering phase function parameter g as a function of shoot albedo ω_{SH}. Shoots are plotted with different colors.

approximation. Indeed, as there is no flat surface which could contribute the Lambertian component, the model does not directly explain the physical scattering process inside the shoot.

The isotropic scattering contribution f_{iso} in the isotropic-Lambertian model is presented in Fig. 5 as a function of total shoot scattering (i.e, shoot albedo ω_{SH}). Generally, all points seem to align on the same straight line crossing the origin of the coordinates (thus indicating a constant fraction of isotropic scattering, f_{iso}/ω_{SH}). However, a more detailed analysis indicated that small between-shoot variations in f_{iso}/ω_{SH} directly correlated with shoot structural variables (results not shown here).

When the Henyey-Greenstein parameter g was fitted for each wavelength and each shoot, it showed a dependence on ω_{SH} (Fig. 6). The theoretical range for g is between -1 and 1, with negative values indicating backward scattering, positive forward scattering and $g = 0$ indicates isotropic scattering (thus, Eq. 3 is a special case of Eq. 4 with $g = 0$). A value at either end of the range, $g \simeq \pm 1$ indicates highly peaked scattering. The g-values in Fig. 6 are strictly negative, but not far from zero. Thus, while shoots are evidently backward-scatterers, the backscatter is not directed into a narrow peak around the hotspot direction. Based on fitting of the Henyey-Greenstein phase function, there is some variation in directional characteristics with shoot albedo (and thus also wavelength). However, the dependence in Fig. 6 is not as explicit as in Fig. 5 and the magnitude of the variation of g with wavelength is of approximately the same magnitude as between-shoot variation in g. This indicates that the isotropic-Lambertian model is better suited for both capturing the general characteristics of a shoot scattering phase function and for describing the wavelength-dependence of the directional distribution of shoot scattering using the presented experimental approach.

Next, we assessed the effect of non-isotropic shoot scattering on the scattering properties of a vegetation layer. For this purpose, a Monte Carlo radiative transfer model (Mõttus and Stenberg, 2008) was parameterized with the shoot scattering parameters described above. We chose two shoot albedos, $\omega_{SH} = 0.1$ and $\omega_{SH} = 0.8$, corresponding to red and near-

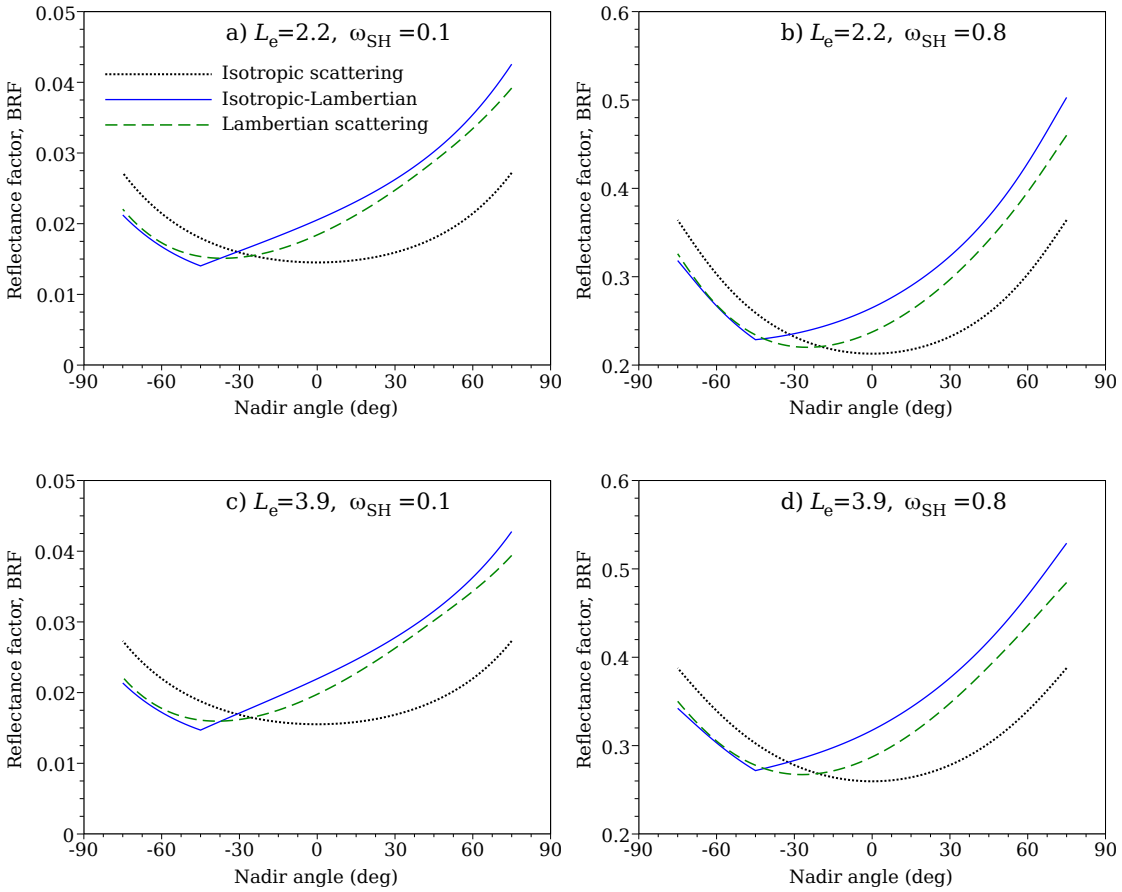

Figure 7: The Bidirectional Reflectance Factor (BRF) of a homogeneous shoot layer as predicted by a Monte Carlo model at two effective LAI values, L_e = 2.2 and L_e = 3.9, in the principal plane. Nadir angle refers to the angle between view direction and the vertical direction. Two phase functions were used in the model for shoot canopies (isotropic, dotted line, and isotropic-Lambertian, solid line) for shoot albedo ω_{SH} = 0.10 and ω_{SH} = 0.80. Additionally, each subplot contains the BRF of a broadleaf canopy with equal L_e (Lambertian scattering, dashed line). Positive nadir angle corresponds to backscatter, solar zenith angle is 45°.

infrared wavelengths, respectively (Fig. 4). Two LAI values were used, LAI = 4.0 and LAI = 7.0. The LAI values correspond to "true LAI" (or hemisurface LAI, Lang, 1991; Chen and Black, 1992; Stenberg, 2006). To describe the dependence of scattering directionality on shoot albedo, we used the best-performing shoot scattering phase function model, isotropic-Lambertian phase function. The spectral dependence of the two components in the model was parameterized as

$$f_{iso} = 0.77\omega_{SH} \quad (6)$$

(see Eq. 5 for definition of f_{iso}) corresponding to the least-squares fit of the data presented in Fig. 5.

To compare the reflectances of similar broadleaf and needle-leaf canopies, we also simulated the reflectance of a horizontally homogeneous leaf canopy. The LAI of the equivalent leaf canopy, however, is considerably smaller than that of the shoot canopy. Instead of true LAI, a more directly comparable quantity (in terms of canopy transmittance, or optical depth) is the effective LAI, L_e. For a homogeneous leaf canopy, L_e = LAI. For a shoot canopy, L_e is obtained by correcting true LAI for within-shoot clumping using the hemispherically-averaged silhouette to total area ratio, $\overline{\text{STAR}}$. Based on the results reported by Rautiainen et al. (2011), we chose $\overline{\text{STAR}}$ = 0.14 as a representative value for the ten shoots. Now, the effective LAI values corresponding to LAI = 4.0 and LAI = 7.0 are L_e = 2.2 and L_e = 3.9, respectively.

For the broadleaf canopy, isotropic leaf normal distribution was used ($G \equiv 0.5$). We set leaf reflectance and transmittance equal to the measured shoot reflectance and transmittance, respectively. Based on our measurements, shoot transmittance forms a fairly constant fraction of total shoot scattering. According to the averaged data, the least squares fit for shoot forward scattering (i.e., shoot diffuse transmittance) is $t_{SH} = 0.38\omega_{SH}$. This is also evident in Fig. 5: shoot transmittance, or forward scattering, constitutes one half of the isotropic component given by Eq. (6). However, the concepts of shoot transmittance and leaf transmittance are not identical. Shoot transmittance is defined as scattering into the forward hemisphere which, in turn, is defined by the direction of incident radiation. Leaf transmittance, on the other hand, is scattering into a hemisphere defined by both incidence direction and the direction of leaf normal.

The bidirectional reflectance factors (BRFs) in the principal

plane obtained from the Monte Carlo simulations are shown in Fig. 7. In addition to the two curves described above (anisotropic shoot scattering using the isotropic-Lambertian model and the Lambertian leaf scattering), the BRF produced by completely isotropic scatterers is presented for comparison. As we modeled the vegetation as a turbid medium model above a completely absorbing soil, all BRF curves are bowl-shaped and monotonously increasing with the view angle ϑ in the backward-scattering direction, $\vartheta > 0$. No hotspot is produced by the model. In contrast, the forward-scattering directions for non-isotropic shoot scattering include a direction of minimum reflectance in the principal plane, a so-called dark spot. In case of the isotropic-Lambertian phase function, the phase function fitting best the measured scattering directionality, the dark spot is very clearly defined. The sharpness of the dark spot is increased by the breaking point in the phase function at scattering angle $(\Omega_{in}, \Omega) = 90°$, a mathematical effect. While the true shoot phase function is undoubtedly more smooth than the isotropic-Lambertian model, the well-expressed dark spot for coniferous canopies is a known phenomenon. After detecting this effect using the space-borne POLDER instrument, Lacaze et al. (2002) and Chen et al. (2003), while not ignoring the possible contribution of shoot scattering anisotropy, attributed this effect mainly to tree-level structure and a higher level of shadow visibility in conifers. While we did not evaluate the effect of larger-level (e.g., branch or tree) structure on canopy BRF, our results (shown in Fig. 7) suggest that shoot scattering phase function may have a considerable contribution to the phenomenon.

Considering the phase functions of a shoot and a leaf, the smaller scattering of the shoots (compared to leaves) in the direction perpendicular the direction of incidence may seem somewhat controversial. Indeed, in a canopy of flat Lambertian leaves with isotropic distribution of leaf normals, the the scattering phase function in the direction Ω has a minimum at $(\Omega_{in}, \Omega) = 90°$ (Ross, 1981). The minimum value of the scattering phase function is a function of the leaf single-scattering albedo ω_L only, $P_L((\Omega_{in}, \Omega) = 90°) = \frac{8}{3\pi}\omega_L$. In contrast, the shoot scattering phase function does not have such a minimum in the darkspot direction. Nevertheless, the value of the shoot scattering phase function at 90° is smaller than that of the leaf canopy: according to Eqs. (5) and (6), $P_{SH}(90°) = 0.77\omega_{SH} < \frac{8}{3\pi}\omega_L$ (taking $\omega_L = \omega_{SH}$), where $\frac{8}{3\pi}\omega_L \simeq 0.85\omega_L$ is the value of $P_L(90°)$.

Another interesting result of our Monte Carlo simulations is that the effect of shoot scattering phase function may, at least in the red spectral region (Fig. 7a,c), be larger than that of a change in LAI. For almost all view angles, especially those in the forward scattering directions ($\vartheta < 0$) in the principal plane, the range of variation of BRF with LAI is of similar to that of BRF variation between the different phase functions. In contrast, the canopy BRFs in near-infrared (Fig. 7b,d), variation of BRF with LAI is large. Naturally, care must be taken when interpreting Fig. 7 as it contains only the signal from shoots. In addition, the forest floor is assumed to be black and canopy structure, except that at shoot level, is ignored.

The back-scattering nature of shoots has been previously suggested by Smolander and Stenberg (2003) and Rochdi et al. (2006) based on Monte Carlo radiative transfer simulations. Neither of the articles report any sharp directional scattering features that would drastically reduce the accuracy of the integration quadrature presented here. In addition, based on the earlier Monte Carlo simulations, the shoot hot spot (which we did not manage to measure in this particular experimental setup) is rather narrow and has no large effect on the value of the shoot scattering coefficient ω_{SH}. A more unexpected finding may be the lack of any strong directional features previously reported by Ross et al. (1994) during measurements of Scots pine shoots. The angular effects, which may originate in specular reflectance on the wax coating of the needles or, alternatively, arise from the special spatial arrangement of needles in the shoot (Nilson and Ross, 1997), may have remained undetected due to a relatively larger distance between integration nodes. Alternatively, they were not properly detected due to insufficient illumination effects (e.g., geometrical setup, internal beam divergence).

In our experiment, we measured ten Scots pine shoots. The small sample naturally limits the possibility to generalize our results to all Scots pine shoots regardless of their size or growth location or other coniferous tree species which have different shoot structures. Another limitation of our study is related to the measurement angles. The set of view directions directions used for measurements is referred to in this article as a "quadrature" since it is optimized for estimating the level of shoot scattering, or the shoot albedo ω_{SH}, not the angular variation of the shoot scattering phase function $P(\Omega_{in} \rightarrow \Omega)$. This is an almost inevitable limitation as the knowledge of the exact value of ω_{SH} is, from application viewpoint, often more important than the knowledge of P_{SH} and is required for a proper normalization of measurement results. Additionally, we fixed all shoots at the same angle to the incident beam: the shoots were irradiated from their largest side. However, this is not necessarily a limitation. Considering the axial symmetry of many shoots and their prolonged shape, photons will most likely hit the shoots in geometry similar to what we used in laboratory. Further, assuming a random distribution of shoot orientation, the particular scattering features of any specific irradiation geometry are averaged. Therefore, for a coniferous shoot canopy, a mean shoot scattering phase function may be used (Nilson and Ross, 1997), similar to the one presented here.

4. Conclusions

We have demonstrated the feasibility of using a high resolution non-imaging spectroradiometer mounted on a laboratory goniometer for measuring shoot scattering phase function. Although the measurements were performed at the sensitivity limit of the spectroradiometer, we conclude that of the three simple phase functions (isotropic, Henyey-Greenstein, and isotropic-Lambertian) tested here, the isotropic-Lambertian phase function matches best the measured shoot scattering directionality. The isotropic-Lambertian phase function models shoot reflectance as a sum of two components. The isotropic component is constant with scattering angle and the Lambertian component, present only in backward scattering, is a lin-

ear function of scattering angle. Further, based on our Monte Carlo radiative transfer simulations, we suggest that asymmetric shoot scattering phase function has a considerable contribution to the high hotspot – darkspot contrast reported for coniferous species in scientific literature.

5. Acknowledgments

We are grateful to Mr. Damien Markulin (University of Zurich) for valuable assistance in setting up the experiment. The research has been funded by University of Helsinki Postdoctoral Funds and Academy of Finland.

References

Atkinson, K., 1982. Numerical-integration on the sphere. Journal of the Australian Mathematical Society Series B – Applied Mathematics 23, 332–347.

Cescatti, A., 1997. Modelling the radiative transfer in discontinuous canopies of asymmetric crowns. II. Model testing and application in a Norway spruce stand. Ecological Modelling 101, 275–284.

Chen, J., Black, T., 1992. Defining leaf area index for non-flat leaves. Plant, Cell & Environment 15, 421–429.

Chen, J., Liu, J., Leblanc, S., Lacaze, R., Roujean, J.L., 2003. Multi-angular optical remote sensing for assessing vegetation structure and carbon absorption. Remote Sensing of Environment 84, 516–525.

Dangel, S., Kneubühler, M., Kohler, R., Schaepman, M., Schopfer, J., Schaepman-Strub, G., Itten, K., 2003. Combined field and laboratory goniometer system – FIGOS and LAGOS, in: Proceedings of International Geoscience and Remote Sensing Symposium (IGARSS), Toulouse, France, IEEE. pp. 4428–4430.

Dangel, S., Verstraete, M., Schopfer, J., Kneubühler, M., Schaepman, M., Itten, K., 2005. Toward a direct comparison of field and laboratory goniometer measurements. IEEE Transactions on Geoscience and Remote Sensing 43, 2666–2675.

Henyey, L.G., Greenstein, J.L., 1941. Diffuse radiation in the Galaxy. Astrophysical Journal 93, 70–83.

Lacaze, R., Chen, J., Roujean, J.L., Leblanc, S., 2002. Retrieval of vegetation clumping index using hot spot signatures measured by POLDER instrument. Remote Sensing of Environment 79, 84–95.

Lang, A., 1991. Application of some of Cauchy's theorems to estimation of surface areas of leaves, needles and branches of plants, and light transmittance. Agricultural and Forest Meteorology 55, 191–212.

Mõttus, M., Stenberg, P., 2008. A simple parameterization of canopy reflectance using photon recollision probability. Remote Sensing of Environment 112, 1545–1551.

MacArthur, A., MacLellan, C., Malthus, T., 2007. The implications of non-uniformity in fields-of-view of commonly used field spectroradiometers, in: Geoscience and Remote Sensing Symposium, 2007. IGARSS 2007. IEEE International, pp. 2890 –2893.

Milton, E., Schaepman, M., Anderson, K., Kneubühler, M., Fox, N., 2009. Progress in field spectroscopy. Remote Sensing of Environment 113, S92–S109.

Nilson, T., Ross, J., 1997. The use of remote sensing in the modeling of forest productivity. Kluwer Academic Publishers, Dordrecht. chapter Modeling radiative transfer through forest canopies: implications for canopy photosynthesis and remote sensing. pp. 23–60.

Oker-Blom, P., Kellomäki, S., 1983. Effect of grouping of foliage on the within-stand and within-crown light regime: Comparison of random and grouping canopy models. Agricultural Meteorology 28, 143–155. Cited By (since 1996) 60.

Rautiainen, M., Mõttus, M., Yáñez Rausell, L., Homolová, L., Malenovský, Z., Schaepman, M., 2011. A note on upscaling from coniferous needle spectral albedo to shoot spectral albedo. Remote Sensing of Environment , in press.

Rochdi, N., Fernandes, R., Chelle, M., 2006. An assessment of needles clumping within shoots when modeling radiative transfer within homogeneous canopies. Remote Sensing of Environment 102, 116–134.

Ross, J., 1981. The Radiation Regime and Architecture of Plant Stands. The Hague: Dr. W. Junk Publishers.

Ross, J., Meinander, O., Sulev, M., 1994. Spectral scattering properties of Scots pine shoots, in: IGARSS '94 - 1994 International Geoscience and Remote Sensing Symposium Volumes 1–4, pp. 1451–1454.

Smolander, S., Stenberg, P., 2003. A method to account for shoot scale clumping in coniferous canopy reflectance models. Remote Sensing of Environment 88, 363–373.

Stenberg, P., 1996. Correcting LAI-2000 estimates for the clumping of needles in shoots of conifers. Agricultural and Forest Meteorology 79, 1–8.

Stenberg, P., 2006. A note on the G-function for needle leaf canopies. Agricultural and Forest Meteorology 136, 76–79.

Stenberg, P., Mõttus, M., Rautiainen, M., 2008. Modeling the spectral signature of forests: application of remote sensing models to coniferous canopies., in: Liang, S. (Ed.), Advances in Land Remote Sensing: System, Modeling, Inversion and Application. Springer-Verlag, pp. 147–171.